

Full-Dynamics Analytical Modeling of Normal Forces for Skid-Steering Mobile Heavy-Duty Manipulators with Actively Articulated Suspension

Alvaro Paz, Mohammad Bahari, and Jouni Mattila

Abstract—This paper presents a geometric approach to calculating the ground reaction normal forces of a four-wheel heavy-duty parallel-serial mobile manipulator in an analytical manner. Such a skid-steering mobile platform is endowed with an actively articulated suspension, thus becoming a rigid multibody system itself. Our solution exploits the wheel’s dynamics decomposition to project the wheels’ internal dynamics and friction forces, preserving all their mechanical effects without hard assumptions. Developing a closed-kinematic chain dynamical analysis, our approach embraces the parallel-serial manipulator and the articulated suspension in a unique screw-theory formulation. Additionally, with respect to previous approaches, our normal forces solutions account for all nonlinear dynamics and accelerations in both the articulated suspension and the wheels. This results in an accuracy enhancement, as demonstrated by a reduction of the average error in normal forces computation by half while traversing uneven terrains when simulating a 7-DoF mobile manipulator with a 2-DoF suspension. We include a losing-contacts robust formulation.

I. INTRODUCTION

Uneven-terrain traversing is a challenging task for heavy-duty manipulators [1], [2]. These mechanisms are commonly powered by hydraulic actuators and are widely employed in forestry, mining, and construction activities [3] requiring tailored modeling and control formulations to address their particular characteristics, such as bulky rigid bodies, relatively low-velocity dynamics, high payload manipulation and wheel-ground dynamics. To reduce the probability of overturning, the control system must consider the modeling of overturning metrics and formulate the appropriate control approaches that monitor and track such metrics to mitigate the overturning events. Also, these wheeled mechanisms can be equipped with active articulated suspension that imposes new challenges for modeling the overturning criteria; however, its control can be used for mechanic stabilization.

Screw theory is a well-established geometric formulation [4], [5] capable of handling the mechanics of complex multibody systems. In this context, the parallel-serial manipulator dynamics have been reported with analytic solutions in [6]–[8]. Moreover, static and dynamic metrics for overturning prevention have been reported. For instance, some of these metrics are, the center-of-mass-based stability angles [9] which considers an active suspension and a serial manipulator, the zero-moment point [10] that is especially common in humanoid robot locomotion, the centroidal momentum [11]

This work was supported by the Business Finland partnership project “Future all-electric rough terrain autonomous mobile manipulators” (Grant #2334/31/2022). Corresponding author: Alvaro Paz.

All authors are with the Faculty of Engineering and Natural Sciences, Tampere University, Tampere, Finland. alvaro.pazanaya@tuni.fi, mohammad.bahari@tuni.fi, jouni.mattila@tuni.fi

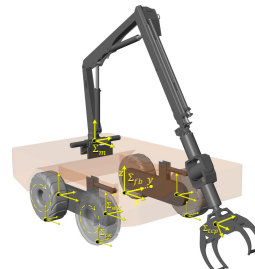


Fig. 1. **Mobile manipulator.** This consists of a heavy-duty parallel-serial manipulator mounted on top of a skid-steering wheeled mobile platform.

to regulate the quantity of the robot motion, and the wheeled mobile manipulator normal forces monitoring [12], [13]. In particular, [13] presented a hybrid approach combining dynamic and quasi-static aspects of a heavy-duty mobile manipulator to calculate the normal forces.

The geometric formulation presented in this work is a direct and considerable enhancement to the ground-reaction normal forces approach reported by [13]. The essential contributions are: (a) the twist and spatial acceleration vectors of the floating base are fully considered without approximations; (b) using a geometric approach, we decompose the dynamic effects acting on the wheels, which helps to project the full internal dynamics of the wheels without any approximation or hard assumption; (c) we include the mechanical analysis of the two-bogies suspension mechanism as a rigid multibody itself, which is essential for considering all dynamic effects on the mobile base and the articulated suspension; (d) Our recursive formulation naturally incorporates external effects, such as the wheels-ground friction forces; (e) we analyze the normal-forces parameter D and propose an extra parameter β to rely on a 4×4 linear system with a unique solution; and (f) we provide a general theorem of a geometric formulation for solving the dynamics in the closed kinematic chains present in the parallel-serial manipulator and in the articulated suspension.

II. HEAVY-DUTY MOBILE MANIPULATOR DYNAMICS

The mobile platform is depicted and described in Fig. 1, where the reference frames for the floating base, manipulator base, and tool center point (TCP) are represented by Σ_{fb} , Σ_m , and Σ_{tcp} , respectively. Additionally, the four wheels follow the nomenclature presented in Fig. 2, where $\Sigma_{w\kappa}$ and $\Sigma_{c\kappa}$ are the wheel and ground-contact reference frames of the κ -th wheel, such that

$$\kappa \in \{FL, RL, FR, RR\} \quad (1)$$

which are the indexes for the front/rear right/left wheels.

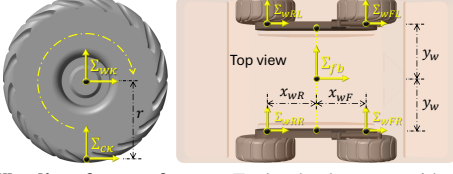


Fig. 2. **Wheel's reference frames.** Each wheel rotates with respect to its Σ_w reference frame, while Σ_c is its corresponding ground-contact frame.

Let us now kinematically and dynamically analyze each of the components of the rigid multibody platform by adopting a geometric formulation based on screw theory. We define the floating base frame Σ_{fb} as the mobile reference frame to express the whole dynamics of the robot, which can be done due to the geometric frame invariance properties. Thus, the frame Σ_{fb} is placed in the middle of the axis that connects both bogies (see Fig. 1). By defining the world's inertial frame as Σ_W , the forward kinematics of Σ_{fb} with respect to Σ_W is represented by the homogeneous transformation matrix G_W^{fb} , which is an element of the Lie group $SE(3)$. Moreover, the Lie algebra associated with the tangent space of this Lie group is $se(3)$, whose elements may be the twist vector ν_{fb} and the spatial acceleration $\dot{\nu}_{fb}$ of the frame Σ_{fb} with respect to Σ_W . The elements G_W^{fb} , ν_{fb} , and $\dot{\nu}_{fb}$ can be retrieved directly from odometry sensors or by time integration of the skid-steering kinematic models from wheels' angular velocities [14], [15].

A. Dynamics of the Closed Kinematic Chain

The parallel-serial manipulator and the two bogies shown in Fig. 1 are endowed with a common closed kinematic chain which has the same kinematic topology. Thus, this section aims to generalize the dynamic analysis of this mechanism depicted in Fig. 3, while the right side indicates the common cases where this mechanism appears in the mobile platform.

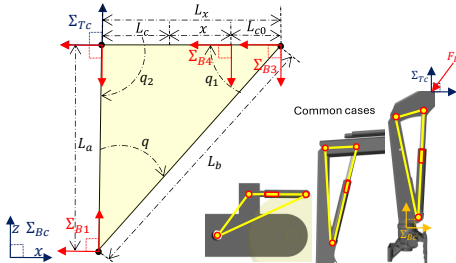


Fig. 3. **Closed kinematic chain.** This mechanism is common in both the parallel-serial manipulator and the articulated suspension mechanism.

The kinematic topology of this 1-DoF mechanism can be analyzed in a plane, and it is defined by four links connected through four joints: three passive rotational joints with attached frames Σ_{B1} , Σ_{B3} , and Σ_{Tc} , and with angular positions θ , θ_1 , and θ_2 , respectively, in addition to an actuated linear joint with an attached frame Σ_{B4} and position x . The origins of the three rotational-joints reference frames generate a triangle where trigonometry can be applied for closure and constraints; such a triangle has internal angles

of q , q_1 , and q_2 , retrieved from x as [6]

$$q = -\arccos\left(\frac{L_x - L_b^2 - L_a^2}{-2L_b L_a}\right) \quad (2)$$

$$q_1 = -\arccos\left(\frac{L_a^2 - L_x^2 - L_b^2}{-2L_x L_b}\right) \quad (3)$$

$$q_2 = -\arccos\left(\frac{L_b^2 - L_x^2 - L_a^2}{-2L_x L_a}\right) \quad (4)$$

where L_a , L_b , and $L_x > 0$ are the lengths of the triangle, and L_x is a function of x as $L_x = L_{c0} + x + L_c$. Moreover, θ , θ_1 , and θ_2 can be obtained from the internal angles as

$$\theta = q + \psi, \quad \theta_1 = q_1 + \psi_1, \quad \theta_2 = q_2 + \psi_2 \quad (5)$$

where ψ , ψ_1 , and ψ_2 are constant offset angles, and through time differentiation of (5), we can compute the joints' angular velocities and accelerations as follows:

$$\dot{\theta} = \dot{q} = k_1 \dot{x}, \quad \ddot{\theta} = \ddot{q} = \dot{k}_1 \dot{x} + k_1 \ddot{x} \quad (6)$$

$$\dot{\theta}_1 = \dot{q}_1 = k_2 \dot{x}, \quad \ddot{\theta}_1 = \ddot{q}_1 = \dot{k}_2 \dot{x} + k_2 \ddot{x} \quad (7)$$

$$\dot{\theta}_2 = \dot{q}_2 = k_3 \dot{x}, \quad \ddot{\theta}_2 = \ddot{q}_2 = \dot{k}_3 \dot{x} + k_3 \ddot{x} \quad (8)$$

where \dot{x} and \ddot{x} are time derivatives of x , and \dot{k}_1 , \dot{k}_2 , and \dot{k}_3 are the time derivatives of k_1 , k_2 , and k_3 ; see [8] for details.

The mechanism in Fig. 3 can be kinematically studied as two serial kinematic chains that start in the base frame Σ_{Bc} and end in the frame Σ_{Tc} . Therefore, based on the elements $G_{fb}^{Bc} \in SE(3)$ and the vectors ν_{Bc} , $\dot{\nu}_{Bc} \in se(3)$ expressed in their local reference frame, the first- and second-order differential kinematics of the first serial chain are as follows:

$$\nu_{B1} = \text{Ad}_{G_{B1}^{Bc}} \nu_{Bc} + s_z \dot{q} \quad (9a)$$

$$\nu_{Tc1} = \text{Ad}_{G_{Tc1}^{B1}} \nu_{B1} \quad (9b)$$

$$\dot{\nu}_{B1} = \text{Ad}_{G_{B1}^{Bc}} \dot{\nu}_{Bc} + s_z \ddot{q} + \text{ad}_{\nu_{B1}} s_z \dot{q} \quad (9c)$$

$$\dot{\nu}_{Tc1} = \text{Ad}_{G_{Tc1}^{B1}} \dot{\nu}_{B1} \quad (9d)$$

For the second serial kinematic chain,

$$\nu_{B3} = \text{Ad}_{G_{B3}^{Bc}} \nu_{Bc} + s_z \dot{q}_1 \quad (10a)$$

$$\nu_{B4} = \text{Ad}_{G_{B4}^{B3}} \nu_{B3} + s_x \dot{x} \quad (10b)$$

$$\nu_{Tc2} = \text{Ad}_{G_{Tc2}^{B4}} \nu_{B4} + s_z \dot{q}_2 \quad (10c)$$

$$\dot{\nu}_{B3} = \text{Ad}_{G_{B3}^{Bc}} \dot{\nu}_{Bc} + s_z \ddot{q}_1 + \text{ad}_{\nu_{B3}} s_z \dot{q}_1 \quad (10d)$$

$$\dot{\nu}_{B4} = \text{Ad}_{G_{B4}^{B3}} \dot{\nu}_{B3} + s_x \ddot{x} + \text{ad}_{\nu_{B4}} s_x \dot{x} \quad (10e)$$

$$\dot{\nu}_{Tc2} = \text{Ad}_{G_{Tc2}^{B4}} \dot{\nu}_{B4} + s_z \ddot{q}_2 + \text{ad}_{\nu_{Tc2}} s_z \dot{q}_2 \quad (10f)$$

where $\text{ad}_{(\nu)} : se(3) \rightarrow \mathbb{R}^{6 \times 6}$ is the Lie bracket operator, $\text{Ad}_{G_i^\lambda} : SE(3) \rightarrow \mathbb{R}^{6 \times 6}$ is the adjoint operator [4], [5] and $s_x, s_z \in se(3)$ correspond to the screw axis of motion defined by

$$s_x = [1 \ 0 \ 0 \ 0 \ 0 \ 0]^\top$$

$$s_z = [0 \ 0 \ 0 \ 0 \ 0 \ 1]^\top$$

The kinematic closure constraint is imposed through the ending frames of both chains Σ_{Tc1} and Σ_{Tc2} as $G_{Bc}^{Tc} = G_{Bc}^{Tc1} = G_{Bc}^{Tc2}$, $\nu_{Tc} = \nu_{Tc1} = \nu_{Tc2}$ and $\dot{\nu}_{Tc} = \dot{\nu}_{Tc1} = \dot{\nu}_{Tc2}$.

The local wrench $F^* \in se^*(3)$ acting on a rigid body is an element of the dual Lie algebra $se^*(3)$ and can be calculated from the controlled Euler-Poincaré equation [16]

$$F^* = M \dot{\nu} - \text{ad}_\nu^*(\mu) \quad (11)$$

where $\boldsymbol{\nu}$ and $\dot{\boldsymbol{\nu}}$ are the twist and spatial acceleration vectors of the rigid body expressed in its local coordinate frame, $\boldsymbol{\mu} \in se^*(3)$ represents the spatial momentum computed as $\boldsymbol{\mu} = \mathbf{M}\boldsymbol{\nu}$, the adjoint operator for the dual Lie algebra is $\text{ad}^*(\boldsymbol{\nu}) : se(3) \rightarrow \mathbb{R}^{6 \times 6}$, and $\mathbf{M} \in \mathbb{R}^{6 \times 6}$ is the symmetric definite positive spatial inertia matrix which is a function of the rigid body's mass, center of mass, and inertia tensor. The four links composing the mechanism have an associated rigid-body inertia expressed in the frames Σ_{Bc} , Σ_{B1} , Σ_{B3} , and Σ_{B4} ; their associated wrenches in local coordinates, namely, \mathbf{F}_{Bc}^* , \mathbf{F}_{B1}^* , \mathbf{F}_{B3}^* , and \mathbf{F}_{B4}^* , are then solved through (11).

Let us now focus on the mechanism on the right side of Fig. 3 to better illustrate the dynamics resolution. In such a mechanism, we assume an external wrench $\mathbf{F}_E \in se^*(3)$ exerted in the frame Σ_{Tc} from successor links in the multibody system. However, the wrench \mathbf{F}_E is decomposed into two parts, namely $\boldsymbol{\eta}_1$ and $\boldsymbol{\eta}_2 \in se^*(3)$, which affect both serial kinematic chains in the mechanism [6]; the following conditions must then be fulfilled:

$$\boldsymbol{\eta}_1 = \alpha_1 \mathbf{F}_E \quad \text{and} \quad \boldsymbol{\eta}_2 = \alpha_2 \mathbf{F}_E \quad (12)$$

where $\alpha_1, \alpha_2 \in [0, 1]$ are known as distribution factors, such that $\alpha_1 + \alpha_2 = 1$. These factors can be found with a geometric approach [17] for dynamics resolution. Moreover, joint actuator dynamics can be calculated with analytic solutions for the inverse [7] and forward dynamics [8]. Since the main target of this study is the normal forces computation, the joint actuator dynamics are not required but the spatial dynamics in the base frame correspond to Σ_{Bc} , which refers to the total wrench \mathbf{F}_{Bc} exerted in Σ_{Bc} from the four rigid bodies and the external wrench.

For notation simplicity, all wrenches are expressed in their local frames; otherwise, this is indicated with the super index (\cdot); thus, the transformation of an element of $se^*(3)$ is

$$\mathbf{F}_A^{(B)} = \text{Ad}_{G_A^B}^* \mathbf{F}_A \quad (13)$$

where $\text{Ad}_{G_A^B}^* : SE(3) \rightarrow \mathbb{R}^{6 \times 6}$ is the adjoint dual operator.

Theorem 1: Let $\mathbf{F}_E \in se^*(3)$ be the external wrench exerted in the reference frame Σ_E and \mathbf{F}_{Bc}^* , \mathbf{F}_{B1}^* , \mathbf{F}_{B3}^* and \mathbf{F}_{B4}^* the local wrenches associated with the rigid bodies of the four-links four-joints 1-DoF mechanism described in Fig. 3. The total wrench \mathbf{F}_{Bc} exerted in the reference frame Σ_{Bc} is the summation of all the wrenches expressed in the frame Σ_{Bc} and it is invariant to the inner distribution wrenches $\boldsymbol{\eta}_1$ and $\boldsymbol{\eta}_2$.

Proof: From equations (12-13), we project the wrenches of both serial chains from local coordinates to the reference frame Σ_{Bc} as follows:

$$\begin{aligned} \mathbf{F}_{Bc} &= \mathbf{F}_{Bc}^* + \text{Ad}_{G_{B1}^{Bc}}^* \mathbf{F}_{B1}^* + \text{Ad}_{G_{B3}^{Bc}}^* \mathbf{F}_{B3}^* + \text{Ad}_{G_{B4}^{Bc}}^* \mathbf{F}_{B4}^* + \mathbf{F}_E^* && \text{First} \\ &+ \text{Ad}_{G_{B3}^{Bc}}^* \mathbf{F}_{B3}^* + \text{Ad}_{G_{B4}^{Bc}}^* \mathbf{F}_{B4}^* + \text{Ad}_{G_E^{Bc}}^* \boldsymbol{\eta}_2 && \text{Second} \\ &= \mathbf{F}_{Bc}^* + \mathbf{F}_{B1}^{*(Bc)} + \mathbf{F}_{B3}^{*(Bc)} + \mathbf{F}_{B4}^{*(Bc)} + \text{Ad}_{G_E^{Bc}}^* (\boldsymbol{\eta}_1 + \boldsymbol{\eta}_2) \\ &= \mathbf{F}_{Bc}^* + \mathbf{F}_{B1}^{*(Bc)} + \mathbf{F}_{B3}^{*(Bc)} + \mathbf{F}_{B4}^{*(Bc)} + \text{Ad}_{G_E^{Bc}}^* \mathbf{F}_E^* (\alpha_1 + \alpha_2) \\ &= \mathbf{F}_{Bc}^* + \mathbf{F}_{B1}^{*(Bc)} + \mathbf{F}_{B3}^{*(Bc)} + \mathbf{F}_{B4}^{*(Bc)} + \mathbf{F}_E^{(Bc)} \end{aligned}$$

B. Heavy-Duty Manipulator Dynamics

The robot manipulator in Fig. 1 is a multibody system composed of a concatenation of serial mechanisms (telescope and spherical wrist) and parallel mechanisms, such as the one presented in II-A; the kinematics of its base reference frame Σ_m is a function of the floating base frame Σ_{fb} , and it is represented by the elements $\mathbf{G}_W^m \in SE(3)$ and $\boldsymbol{\nu}_m, \dot{\boldsymbol{\nu}}_m \in se(3)$. Additionally, the commanded configurational vector is denoted by $\mathbf{q}_m \in \mathbb{R}^{n_r}$ and the joint velocity and acceleration vectors as $\dot{\mathbf{q}}_m, \ddot{\mathbf{q}}_m \in \mathbb{R}^{n_r}$, where n_r is the manipulator's DoF. By performing a forward recursion from Σ_m to Σ_{tcp} with the twist and spatial acceleration expressions (9) and (10), the kinematic elements $\mathbf{G}_W^{tcp} \in SE(3)$ and $\boldsymbol{\nu}_{tcp}, \dot{\boldsymbol{\nu}}_{tcp} \in se(3)$ can then be calculated. Furthermore, by using *Theorem 1* in a dynamic backward recursion from Σ_{tcp} to Σ_m , the manipulator dynamics are computed as the total wrench exerted from the manipulator to the mobile platform \mathbf{F}_m . This wrench, according to *Theorem 1*, is the summation of all the local wrenches \mathbf{F}_i^* associated with the rigid bodies i in the manipulator expressed in the reference frame Σ_m as:

$$\mathbf{F}_m = \sum_i \text{Ad}_{G_i^m}^* \mathbf{F}_i \quad (14)$$

C. Actively Articulated Suspension Dynamics

The mobile base in Fig. 1 is supported by two bogies connected through two closed kinematic chains, such as the one presented in Section II-A. The bogies are actuated by means of two linear actuators with positions, velocities, and accelerations $\mathbf{x}_s, \dot{\mathbf{x}}_s, \ddot{\mathbf{x}}_s \in \mathbb{R}^2$. Since the kinematics of frame Σ_{fb} are known, the transformation matrices, twists, and spatial velocities of all the reference frames in the bogies are computed through (9) and (10). In addition, by recalling the *Theorem 1*, the joint actuator dynamics do not need to be computed. The dynamical effects of the base and bogies are then represented by the summation of the rigid body wrenches \mathbf{F}_B , expressed in the reference frame Σ_{fb} as

$$\mathbf{F}_B = \mathbf{F}_{Ba}^{*(Bc)} + \sum_{j \in \{R, L\}} \left(\mathbf{F}_{Bo_j}^{*(Bc)} + \mathbf{F}_{Cy_j}^{*(Bc)} + \mathbf{F}_{Pi_j}^{*(Bc)} \right) \quad (15)$$

where \mathbf{F}_{Ba}^* is the local wrench of the base, $\mathbf{F}_{Bo_j}^*$ is the bogie wrench, and $\mathbf{F}_{Cy_j}^*$ and $\mathbf{F}_{Pi_j}^*$ are the wrenches associated with the cylinder and piston components of the linear actuators. The index j iterates for the right- and left-sided bogies.

D. Wheel-Ground Mechanical Interaction

Each bogie has two-wheel reference frames Σ_{wF} and Σ_{wR} for the front and rear wheels' motion. According to Fig. 2, each wheel mechanism is a one-DoF revolute and actuated joint that rotates around the Y axis of its Σ_w frame. The angular joint positions, velocities, and accelerations of the wheels are denoted by $\mathbf{q}_w, \dot{\mathbf{q}}_w, \ddot{\mathbf{q}}_w \in \mathbb{R}^2$ for the right and left wheels. Each wheel has an associated spatial inertia matrix $\mathbf{M}_{w\kappa}$; thus, its local wrench $\mathbf{F}_{w\kappa}^*$ is directly computed from (11), where κ is the index for the four wheels, see (1). On the other hand, each wheel has a contact reference frame Σ_c , where the wheel-ground mechanical interaction is resolved.

The terrain reaction forces are denoted by the wrench \mathbf{F}_r , and it is expressed in Σ_c frame; additionally, the terrain friction forces \mathbf{F}_a act directly on this frame. Thus, the forces acting on the wheel frame Σ_w are

$$\mathbf{F}_w^* + \text{Ad}_{G_{c^w}}^* (\mathbf{F}_r + \mathbf{F}_a) \quad (16)$$

and the full-dynamics contribution from the four wheels are expressed in the floating-base reference frame Σ_{fb} as

$$\mathbf{F}_w = \sum_{\kappa} \text{Ad}_{G_{w\kappa}^{fb}}^* \left(\mathbf{F}_{w\kappa}^* + \text{Ad}_{G_{c\kappa}^{w\kappa}}^* (\mathbf{F}_{r\kappa} + \mathbf{F}_{a\kappa}) \right) \quad (17)$$

III. GROUND REACTION NORMAL FORCES

The full dynamics of the mobile heavy-duty manipulator with articulated suspension and ground reaction forces can be resolved in the floating base reference frame Σ_{fb} as follows

$$\text{Ad}_{G_m^{fb}}^* \mathbf{F}_m + \mathbf{F}_B + \mathbf{F}_w = \mathbf{0} \quad (18)$$

where \mathbf{F}_m contains the manipulator dynamics according to (14), \mathbf{F}_B contains the base and suspension dynamics including bogies and cylinders according to (15), and \mathbf{F}_w contributes the wheel and ground interaction effects, as expressed by (17). Before proceeding to the analytic solutions for the normal forces, let us make some assumptions.

- **Skid-steering wheels:** The wheels' motion corresponds to a non-holonomic skid-steering mobile platform; thus, they do not have direct steering nor heading control.
- **Equidistance:** The wheels' reference frames $\Sigma_{w\kappa}$ are equidistant with respect to the Y axis of the floating base frame Σ_{fb} .
- **Homogeneous wheels:** The wheels have the same radius. Nonetheless, inertial properties can be different.
- **One contact:** The wheels are assumed to make contact at just one point, which is the origin of the frame Σ_c .

The wheels' expression (17) can be reformulated as

$$\mathbf{F}_w = \sum_{\kappa} \text{Ad}_{G_{w\kappa}^{fb}}^* \left(\mathbf{F}_{w\kappa}^* + \text{Ad}_{G_{c\kappa}^{w\kappa}}^* \mathbf{F}_{a\kappa} \right) + \sum_{\kappa} \text{Ad}_{G_{c\kappa}^{fb}}^* \mathbf{F}_{r\kappa} \quad (19)$$

which allows us to decompose the wheels' dynamical effects and helps to preserve the full dynamics of the wheels $\mathbf{F}_{w\kappa}^*$ and the friction forces without any assumption or approximation. Therefore, combining expressions (18) and (19) yields

$$\sum_{\kappa} \text{Ad}_{G_{w\kappa}^{fb}}^* \text{Ad}_{G_{c\kappa}^{w\kappa}}^* \mathbf{F}_{r\kappa} = \mathbf{F}_{\Xi} \quad (20)$$

where \mathbf{F}_{Ξ} is the wrench computed as

$$\mathbf{F}_{\Xi} = - \sum_{\kappa} \text{Ad}_{G_{w\kappa}^{fb}}^* \left(\mathbf{F}_{w\kappa}^* + \text{Ad}_{G_{c\kappa}^{w\kappa}}^* \mathbf{F}_{a\kappa} \right) - \text{Ad}_{G_m^{fb}}^* \mathbf{F}_m - \mathbf{F}_B$$

A. Linear Algebra for Analytic Solutions

Let us analyze the LHS of the expression (20). According to Fig. 2, the position vectors of the wheels' reference frames $\Sigma_{w\kappa}$ with respect to the floating base frame Σ_{fb} are

$$\mathbf{p}_{fb}^{wFL} = [x_{wF} \quad y_w \quad z_w]^\top \quad (21a)$$

$$\mathbf{p}_{fb}^{wRL} = [-x_{wR} \quad y_w \quad z_w]^\top \quad (21b)$$

$$\mathbf{p}_{fb}^{wFR} = [x_{wF} \quad -y_w \quad z_w]^\top \quad (21c)$$

$$\mathbf{p}_{fb}^{wRR} = [-x_{wR} \quad -y_w \quad z_w]^\top \quad (21d)$$

and the wheels' frames and the floating base frame are aligned as follows: $\mathbf{R}_{fb}^{w\kappa} = \mathbf{I}_3 \in SO(3)$. Thus the transformation matrices $\mathbf{G}_{fb}^{w\kappa}$ are parameterized by the pairs $(\mathbf{p}_{fb}^{w\kappa}, \mathbf{I}_3)$ and the adjoint dual operator $\text{Ad}_{G_{w\kappa}^{fb}}^*$ has the inner shape

$$\text{Ad}_{G_{w\kappa}^{fb}}^* = \begin{bmatrix} \mathbf{I}_3 & \mathbf{0}_3 \\ [\mathbf{p}_{fb}^{w\kappa}] & \mathbf{I}_3 \end{bmatrix}^\top \quad (22)$$

where $[\mathbf{p}] : \mathbb{R}^3 \rightarrow so(3)$ is a skew-symmetric matrix, and $so(3)$ is the associated Lie algebra of $SO(3)$.

In a general form, we set the contact frames' positions with respect to the wheels' frames as follows:

$$\mathbf{p}_{w\kappa}^{c\kappa} = [x_c \quad 0 \quad r]^\top \quad (23)$$

where r is the wheels' radius depicted in Fig. 2, and x_c takes into account the contact frame displacement in the X axis. In a similar manner, $\mathbf{G}_{w\kappa}^{c\kappa}$ are parameterized by the pairs $(\mathbf{p}_{w\kappa}^{c\kappa}, \mathbf{I}_3)$, and the adjoint operator $\text{Ad}_{G_{w\kappa}^{c\kappa}}^*$ has a similar shape to (22).

We denote the ground reaction wrenches as follows:

$$\mathbf{F}_{r\kappa} = [f_{x\kappa} \quad f_{y\kappa} \quad f_{z\kappa} \quad f_{mx\kappa} \quad f_{my\kappa} \quad f_{mz\kappa}]^\top \quad (24)$$

where $f_{x\kappa}$, $f_{y\kappa}$, and $f_{z\kappa}$ are the linear forces and $f_{mx\kappa}$, $f_{my\kappa}$ and $f_{mz\kappa}$ are the angular torques. Additionally, for a simplified notation, we define the sum of components in X axes as $\mathbf{f}_x = \sum_{\kappa} f_{x\kappa}$. Following this notation, the summation of forces in the Y axes is $\mathbf{f}_y = \sum_{\kappa} f_{y\kappa}$ and so on for the Z axes and angular components. Thus, the LHS of expression (20) is

$$\begin{bmatrix} \mathbf{f}_x \\ \mathbf{f}_y \\ \mathbf{f}_z \\ \mathbf{f}_{mx} + (r - z_w)\mathbf{f}_y + y_w(f_{zFL} - f_{zFR} - f_{zRR} + f_{zRL}) \\ \mathbf{f}_{my} + (z_w - r)\mathbf{f}_x - x_{wF}(f_{zFL} + f_{zFR}) + x_{wR}(f_{zRR} + f_{zRL}) - x_c \mathbf{f}_z \\ \text{Not a function of } f_{z\kappa} \end{bmatrix}$$

which implies, from RHS of (20), that $\mathbf{f}_x = \mathbf{F}_{\Xi(1)}$ and $\mathbf{f}_y = \mathbf{F}_{\Xi(2)}$, where $\mathbf{F}_{\Xi(\cdot)}$ refers to a component of \mathbf{F}_{Ξ} . If we neglect the torque components, namely, $\mathbf{f}_{mx} = 0$ and $\mathbf{f}_{my} = 0$, the last expression and (20) generate a 3×4 linear system $\mathbf{A}\mathbf{x} = \mathbf{b}$ where

$$\mathbf{A}\mathbf{x} = \begin{bmatrix} f_{zFL} + f_{zFR} + f_{zRR} + f_{zRL} \\ y_w(f_{zFL} - f_{zFR} - f_{zRR} + f_{zRL}) \\ -x_{wF}(f_{zFL} + f_{zFR}) + x_{wR}(f_{zRR} + f_{zRL}) - x_c \mathbf{f}_z \end{bmatrix}_{3 \times 1} \quad (25)$$

$$\mathbf{A} = \begin{bmatrix} 1 & 1 & 1 & 1 \\ y_w & -y_w & -y_w & y_w \\ -x_{wF} - x_c & -x_{wF} - x_c & x_{wR} - x_c & x_{wR} - x_c \end{bmatrix}_{3 \times 4} \quad (26)$$

$$\mathbf{x} = [f_{zFL} \quad f_{zFR} \quad f_{zRR} \quad f_{zRL}]_{4 \times 1}^\top \quad (27)$$

$$\mathbf{b} = \begin{bmatrix} \mathbf{F}_{\Xi(3)} \\ \mathbf{F}_{\Xi(4)} - (r - z_w)\mathbf{F}_{\Xi(2)} \\ \mathbf{F}_{\Xi(5)} - (z_w - r)\mathbf{F}_{\Xi(1)} \end{bmatrix}_{3 \times 1} \quad (28)$$

To generate a 4×4 system to be solved with a matrix inversion, works such as [13] included an extra equation

from an empirical normal forces distribution assumption, expressed as follows:

$$\begin{bmatrix} D-1 & 1-D & -D & D \end{bmatrix}_{1 \times 4} \mathbf{x} = \beta \quad (29)$$

with $D \in [0, 1]$ and $\beta = 0$. However, selecting an appropriate value for D and β depends directly in the geometry and complexity of the platform under study. In order to mitigate the subjectivity on the selection of these factors we perform an optimization study based on simulation data to enhance the normal forces' accuracy. Such optimization penalizes the differences among the analytical normal forces computation and the signals retrieved from contact block sensors and is represented by the following unconstrained nonlinear programming problem

$$\underset{D, \beta}{\text{minimize}} \quad f = \frac{1}{2} \sum_{\kappa \in \{FR, FL, RR, RL\}} \left(f_{z\kappa}(D, \beta) - \hat{f}_{z\kappa} \right)^2 \quad (30)$$

where $f_{z\kappa}(D, \beta)$ is the analytical normal forces computation described in this section and $\hat{f}_{z\kappa}$ is the signal from contact blocks in simulation.

B. Losing Contact with the Terrain

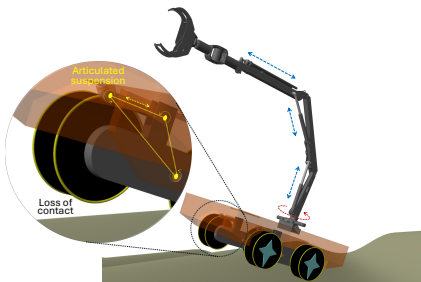


Fig. 4. **Losing the wheel-ground contact.** It is challenging to guarantee a continuous four-wheel contact when traversing uneven terrain.

While traversing rough terrain, the mobile platform has higher probability of temporary loose contact with the ground (see Fig. 4), which can be a source of considerable inaccuracies. Moreover, if at least three wheels are in contact, then Boolean information of contacts can be introduced to generate a 3×3 linear system with (25-27). A zero flag-of-contact can be used to neglect the corresponding column in \mathbf{A} and the row in \mathbf{x} associated with the wheel that has lost contact. For instance, if the wheel FL loses contact, then the first column of \mathbf{A} and the first row of \mathbf{x} must be deleted. This remains in a linear system with a unique solution that does not affect the accuracy of the three wheels in contact.

IV. NUMERICAL SIMULATIONS AND RESULTS

For numerical verification, we simulated traversing motions of the platform presented in Fig. 1 on the MATLAB physic engine Simscape. We also use the Spatial Contact block of Simulink to simulate the wheels-ground interaction and retrieve normal forces signals to use as ground truth. Also, we retrieve from this block friction forces $\mathbf{F}_{a\kappa}$ to include in (17) and Boolean contact signals. First, we simulate a 25 [s] traversing on flat terrain and compare the results against the solutions in [13], see Figs. 5 and 6

for forces and error graphs. Motion commands for the 7-DoF manipulator and the 2-DoF suspension are provided as sinusoidal functions of time while the wheels' motion is $\mathbf{q}_w = \mathbf{b}(t - \sin(t))$, $\dot{\mathbf{q}}_w = \mathbf{b}(1 - \cos(t))$ and $\ddot{\mathbf{q}}_w = a\mathbf{b}\sin(t)$ where $a = 35$ and $\mathbf{b} = [0.9; 0.8]\pi$. The average absolute errors in Fig. 6 is 4.84 [%] for the solution reported in [13] and 2.02 [%] for our full dynamics approach.

Also, we perform a 40 [s] rough terrain traversing with similar manipulator and suspension motion commands and parameters $a = 30$ and $\mathbf{b} = [0.15; 0.15]\pi$ for the wheels' motion. Figs. 7 and 8 depict the normal forces during time and its average error. The uneven terrain has a maximum slope of 26.7° and the average errors in force computation are 9.46 [%] for the solution in [13] and 5.0 [%] for ours.

Additionally, we perform a numerical optimization of parameters D and β of (29) by penalizing the normal forces deviation from the ground truth signals. Fig. 9 shows their optimal values during time which additionally reduced from 2.02 [%] to 0.42 [%] the average error on flat terrain traversing. Notice that for this specific robotic platform the optimal value of D^* oscillates between 1.4 and 1.6, and the optimal value of β^* between -4k and 0. For experimentation purposes this optimization can be performed with real sensors data which probably can help to increase the accuracy in normal forces computation. Moreover, the losing contact method described in III-B is simulated on a 200 [s] rough terrain traversing where the considerable terrain slope (maximum of 26.7°) results in frequent contact loose in all wheels. Fig. 10 illustrates the normal forces. The lines in blue are the ground truth from the Spatial Contact block and the green lines are our robust algorithm which monitors the loss of contact. Note that both signals of normal forces are sensitive to the transition between losing contact and the impact when recovering the contact in each wheel.

V. CONCLUSIONS

Relying on the screw theory formalism, we presented a theorem that generalizes the dynamics resolution of a class of closed kinematic chain and a complete mathematical approach for normal forces computation which takes into account the nonlinear full dynamics of manipulator, articulated suspension and wheels. We validated through numerical simulation our approach in comparison with state-of-the-art solutions [13]. The reported results demonstrate an accuracy improvement by reducing the error in normal forces from 4.84 [%] to 2.02 [%] and from 9.46 [%] to 5.0 [%] for flat and uneven terrains traversing. According to these results our solution has better performance in high-acceleration motions and considerable slopes in the terrain. We equipped our approach with parameters optimization, that reduced the forces error to 0.4 [%] on a flat terrain, and an automatic feature in our algorithm to cope with the loss of contact. Future work is targeted to include this normal forces approach into whole-body optimal controls for real-time experimentation.

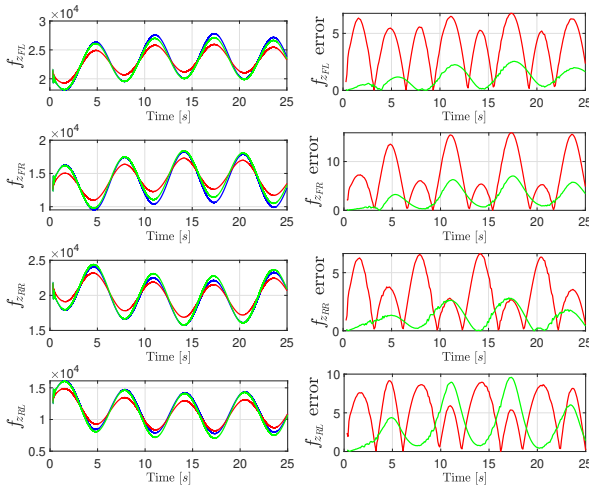


Fig. 5. Normal forces on flat terrain. Blue lines are the Simscape forces, red ones are the quasi dynamic and green lines are our full dynamic solution.

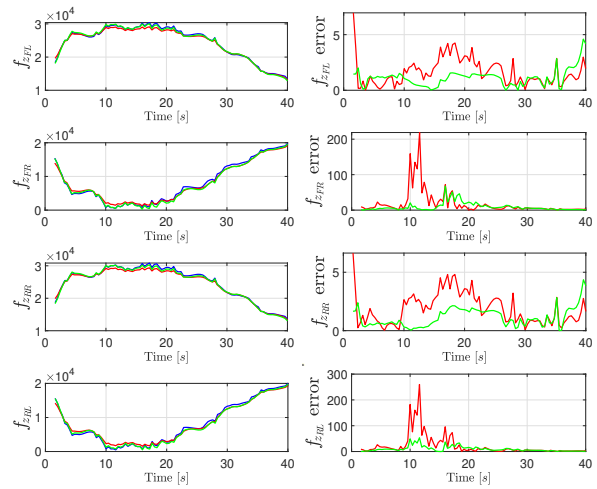


Fig. 6. Absolute force error on flat terrain. Blue lines are the Simscape errors, red ones are the quasi dynamic and green lines are our full dynamic solution.

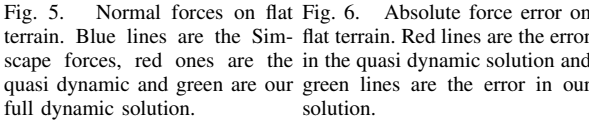


Fig. 7. Forces on rough terrain. Blue lines are the Simscape forces, red ones are the quasi dynamic and green lines are our full dynamic solution.

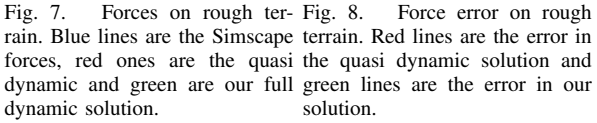


Fig. 8. Force error on rough terrain. Blue lines are the Simscape errors, red ones are the quasi dynamic and green lines are our full dynamic solution.

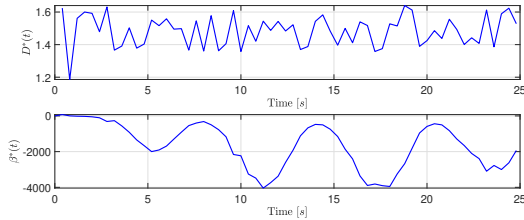


Fig. 9. Optimal values of D and β during flat terrain traversing. This optimization is described by the cost function (30) and includes data from contact blocks in simulation.

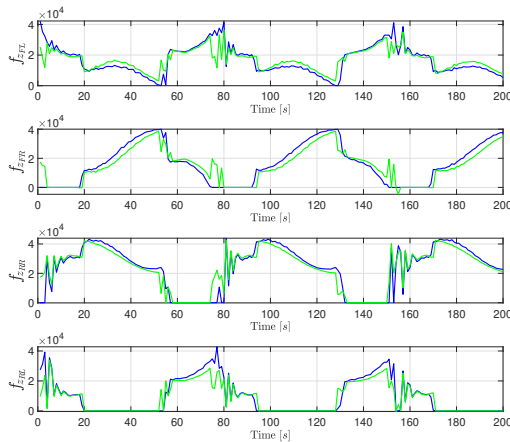


Fig. 10. Contact-loss robust computation of rear normal forces.

REFERENCES

- [1] Liyana Ramli, Z. Mohamed, Auwalu M. Abdullahi, H.I. Jaafar, and Izzuddin M. Lazim. Control strategies for crane systems: A comprehensive review. *Mechanical Systems and Signal Processing*, 95:1–23, 2017.
- [2] Jouni Mattila, Janne Koivumäki, Darwin G Caldwell, and Claudio Semini. A survey on control of hydraulic robotic manipulators with projection to future trends. *IEEE/ASME Transactions on Mechatronics*, 22(2):669–680, 2017.
- [3] Ryan Luke Johns, Martin Wermelinger, Ruben Mascaro, Dominic Jud, Ilmar Hurkkens, Lauren Vasey, Margarita Chli, Fabio Gramazio, Matthias Kohler, and Marco Hutter. A framework for robotic excavation and dry stone construction using on-site materials. *Science Robotics*, 8(84):eabp9758, 2023.
- [4] Kevin M Lynch and Frank C Park. *Modern robotics*. Cambridge University Press, 2017.
- [5] J.-M. Selig. *Geometric Fundamentals of Robotics*. Springer, New York, 2005.
- [6] Wen-Hong Zhu. *Virtual decomposition control: toward hyper degrees of freedom robots*, volume 60. Springer Science & Business Media, 2010.
- [7] Goran R Petrović and Jouni Mattila. Mathematical modelling and virtual decomposition control of heavy-duty parallel–serial hydraulic manipulators. *Mechanism and Machine Theory*, 170:104680, 2022.
- [8] Paz Alvaro and Jouni Mattila. Analytical forward dynamics modeling of linearly actuated heavy-duty parallel–serial manipulators. *arXiv preprint arXiv:2403.08524*, 2024.
- [9] Karl Iagnemma, Adam Rzepniewski, Steven Dubowsky, and Paul Schenker. Control of robotic vehicles with actively articulated suspensions in rough terrain. *Autonomous Robots*, 14:5–16, 2003.
- [10] Miomir Vukobratović and Branislav Borovac. Zero-moment point—thirty five years of its life. *International journal of humanoid robotics*, 1(01):157–173, 2004.
- [11] David E Orin, Ambarish Goswami, and Sung-Hee Lee. Centroidal dynamics of a humanoid robot. *Autonomous Robots*, 35(2-3):161–176, 2013.
- [12] Marco Hutter, Philipp Leemann, Stefan Stevsic, Andreas Michel, Dominic Jud, Mark Hoepflinger, Roland Siegwart, Ruedi Figi, Christian Caduff, Markus Locher, et al. Towards optimal force distribution for walking excavators. In *2015 international conference on advanced robotics (ICAR)*, pages 295–301. IEEE, 2015.
- [13] Goran R Petrović and Jouni Mattila. Analytic solutions for wheeled mobile manipulator supporting forces. *IEEE Access*, 10:43235–43255, 2022.
- [14] Luca Caracciolo, Alessandro De Luca, and Stefano Iannitti. Trajectory tracking control of a four-wheel differentially driven mobile robot. In *Proceedings 1999 IEEE international conference on robotics and automation (Cat. No. 99CH36288C)*, volume 4, pages 2632–2638. IEEE, 1999.
- [15] Krzysztof Kozłowski and Dariusz Pazderski. Modeling and control of a 4-wheel skid-steering mobile robot. *International journal of applied mathematics and computer science*, 14(4):477–496, 2004.
- [16] Jerrold E Marsden and Tudor S Ratiu. *Introduction to mechanics and symmetry: a basic exposition of classical mechanical systems*, volume 17. Springer Science & Business Media, 2013.
- [17] Janne Koivumäki, Wen-Hong Zhu, and Jouni Mattila. Addressing closed-chain dynamics for high-precision control of hydraulic cylinder actuated manipulators. In *Fluid Power Systems Technology*, volume 51968, page V001T01A018. American Society of Mechanical Engineers, 2018.